Green Synthesis of ZnO and Ag-ZnO Nanoparticles using Macrotyloma Uniflorum: Evaluation of Antibacterial Activity

Raghavendra K. Sali[1,2], Malatesh S. Pujar[1], Shivaprasadagouda Patil[1,2], Ashok H. Sidarai[1,]*

In this work, using *Macrotyloma Uniflorum* leaves an affordable and eco-friendly, ZnO and Ag-ZnO metal oxide nanoparticles were reported. Ensuing ZnO and Ag-ZnO nanoparticles were characterized by UV–visible spectroscopy, FT-IR Spectroscopy, X-ray diffraction, Scanning Electron Microscopy with Energy Dispersive Spectroscopy, Transmission Electron Microscopy, and Dynamic Light Scattering. The green synthesized ZnO and Ag-ZnO nanoparticles comprise an average size of about 120.16 nm and 91.17 nm respectively. The minimum inhibitory concentrations (MIC) of these ZnO and Ag-ZnO nanoparticles and mixtures thereof, Ag-ZnO, were determined on *B.subtilis, Streptococci* and *E.coli* cultures. MIC and their antimicrobial activity were studied in vitro; both types of nanoparticles showed high antibacterial activity. Also, it has shown excellent results with MIC value of 62.5 µg/ml for antibacterial activity against ZnO and Ag-ZnO nanoparticles. The Ag-ZnO nanoparticles were shown better antimicrobial effect than the ZnO nanoparticles. So, we can strongly suggest these green synthesized nanoparticles as a potent agent for biological applications.

Introduction

Metal oxides are an important class of engineered nanoparticles, because they are widely used in cosmetics and sunscreens, self-cleaning coatings and textiles [1,2]. Carlos. A. Martinez Synthesized the Biological quantum dots [3]. Robert G. Thorne, *et. al.,* in 2005 worked on the II-IV groups (CdSe, ZnS and CdTe) and IV-VI groups (PbSe and PbS) nanoparticles in brain extracellular space (ECS) [4]. Nath. *et. al.,* in 2013 observed the reduction of hazardous waste generation and antimicrobial activities using biosynthesized Ag and Zn metal nanoparticles [5]. M Darroudi, *et. al.,* reported green and biosynthesized nanoceria to reduce the cytotoxic effect on neuro2A cell lines [6]. Our interest is to diverse from applied science ranging from material science to biotechnology. We observed that some metal oxides suits for their particular applications. That is because of their distinctive physicochemical properties of metal oxides and these properties are mainly depending on size and surface to volume ratio of the nano materials [7,8].

Various metal oxide clusters have been explored for optoelectrical applications [9–12]. Among them, zinc oxide nanoparticles (NPs) are extensively studied because of its high thermodynamic stability, chemically inertness, economically cheap, the direct bandgap of ~ 3.37eV at room temperature and with large binding energy of 60meV, makes them perfect candidates to recruit them in designing the optoelectronic materials [13–15]. The pristine ZnO NPs exhibit weak to moderate optical activity due to the minor point defects arising from the oxygen vacancy and or with the defects including their arrangement in their respective crystal lattice positions. Hence, the optoelectrical property of ZnO NPs can be tuned by the addition of dopant and this dopant must possess n-type and p-type states. In this contest, the silver element plays a significant role as a p-type dopant because of its easy solubility, high ionic size and minimum orbital energy. The 4d and 2p orbital of Ag and O respectively overlap to form an impurity band, which further shifts the Fermi levels towards the valence band thus minimizing the energy gap.

Owing to their eco-friendliness and compatibility for pharmaceuticals and biomedical applications, the bio-

[1]Department of studies in Physics,
Karnatak University Dharwad 580 003, Karnataka, India
[2]Department of Physics, J S S Arts, Science and Commerce College, Gokak 591 307, Karnataka, India

*Corresponding author:
E-mail: ashok_sidarai@rediffmail.com

based synthesis of nanoparticles offers numerous benefits as they use less toxic chemicals in the synthesis protocol [16,17]. In bio-based synthesis of nanoparticles naturally occurring reagents such as a biodegradable polymer, plant extract, and microorganisms are used for the synthesis of nanoparticles. There are phytochemicals present in plants such as terpenoids, flavones, and substituted ketones, aldehydes, amides, carboxylic acids, these phytochemicals are treated with metal ion solution which acts as reducing and capping agents to form nanoparticles [18-21].

Macrotyloma Uniflorum is a legume shrub usually grows in marginal soils of dry lands of western ghats and used to feed for cattle and horses hence commonly known as horse gram. Grown in moderate warm and dry climatic condition with low rainfall, it is extremely drought resistant [22,23]. It was used in ancient traditional medicine culture for treating hemorrhoids, tumors, inflammation, liver problems, and many more. The aqueous extract of leaf was known to consist of polyphenols (reducing agent) and flavonoids, tannin (capping agents) compounds [24-26]. The reason for the selection of *Macrotyloma Uniflorum* is due to the presence of polyphenols, which acts as a reducing agent for the preparation of ZnO and Ag-doped ZnO nanocomposites. Various methods are available for the synthesis of metal oxide and doped metal oxide nanoparticles of different size, shape, structure, and morphology [27]. In the present investigation, we report the synthesis of ZnO and Ag-ZnO nanocomposites using the aqueous leaf extract of *Macrotyloma Uniflorum* in ambient conditions. This biosynthesis method of NPs is very simple, economical, and eco-friendly [28]. The biosynthesized NPs from this plant gained less attention, this is the first report on phyto-synthesis of NPs using *Macrotyloma Uniflorum* and these NPs are characterized by various spectroscopic techniques. The change in optical properties and morphological effect of dopant Ag on ZnO is also studied.

Further, observed unique characteristics of synthesized ZnO nanoparticles lead us to biological applications. Zinc oxide (ZnO) is a versatile semiconductor material; it has been attracting attention because of the commercial demand for blue and UV regions operating optoelectronic devices. Like other groups of metal oxides the ZnO and Ag-ZnO also exhibits antibacterial activity, to achieve this few have scaled down the size of the materials and we extended the same to ZnO and Ag-ZnO nanoparticles [25,26]. ZnO and Ag-ZnO nanoparticles exhibit a higher degree of efficiency in medical treatments with the ability to surpass the therapeutic indices of some commonly used chemotherapeutic agents. The benefit of using inorganic oxides such as zinc oxide or doped oxide as antimicrobial agents is, they contain mineral elements which are essential to humans and exhibit strong activity even when administered in small units [29]. Ag-ZnO nanoparticles exhibit strong antibacterial activities than ZnO nanoparticles on a broad spectrum of bacteria and act as a potent agent.

Experimental

Materials used

All the chemicals used are of analytical grade and are used without any further purification. The plant leaves (leaf of *Macrotyloma Uniflorum*) was collected in fields of Gandinagar village near Shikaripura and authenticated at the department of Botany, Karnatak University Dharwad. $ZnSO_4$ (99%, Sigma chemicals India) and $AgNO_3$ (99.9%) Sigma Aldrich, India).

Preparation of leaf extract using macrotyloma uniflorum

10g of *Macrotyloma Uniflorum* leaf was weighed and washed several times with distilled water, chopped into small pieces then placed in RB flask containing 100 ml doubled distilled water and maintained under 50-60° C temperature for an hour. Later, the solution was allowed to cool at room temperature, filtered through Whatman's filter paper no. 1. Beyond filtering, the aqueous plant extract was obtained and stored at 4 °C, which was further used in the synthesis of nanoparticles.

Synthesis of pure and Ag doped Zinc Oxide nanoparticles by co-precipitation method

In a round bottom flask, 20 ml of the aqueous leaf extract of *Macrotyloma Uniflorum* leaf was taken and stirred for 20 min at 70° C. 0.1 ml of 3M $ZnSO_4$ was added to the solution. Then by stirring it continuously, NaOH solution was added to maintain pH 12. Finally, the white precipitate which was a source of the pure compound was obtained. This was further subjected to centrifugation in order to remove the supernatant using ethanol. Later, the obtained materials were annihilated for 10 h at 60 °C in a hot air oven. The same method has been followed to synthesis Ag-doped NPs. 20 ml of plant extract was stirred at a temperature of 70°C for 15 min and 3M of 0.1 ml $ZnSO_4$ and 0.05M of 2ml $AgNO_3$ was added dropwise one after another. Finally, the NaOH solution was added. The obtained precipitation was washed several times using distilled water and once by ethanol, annihilated at 60° C for 12h using hot air oven.

Material characterizations

Optical properties of nanocomposites were recorded using UV-visible spectral analysis (Beckman-Coulter DU-730 UV-Vis Spectrophotometer, USA) with wavelength (λ) scan from 200 to 800 nm in different time intervals. The functional group analysis for the prepared nanocomposites was analyzed using FT-IR (PIKE Technologies, Spectrum Two, USA) at 4000-400 cm^{-1} range of wavelength. The powder X-ray diffraction was done by RIGAKU X-ray Diffractometer, model-smart lab 3kW with Cu Kα source at 2θ angle probed 10°-80°. Fine powder of ZnO and Ag-ZnO were placed in a platen in a different time and scanned to detect the width of XRD peaks at a rate of 3°/min and the average size of the nanocomposites was

Advanced Materials Letters

www.vbripress.com/aml

![IAAM logo]

Advancement of Materials
to Global Excellence

www.iaamonline.org

estimated using De-Broglie Equation (nλ = 2dsinΘ). The morphological structure and size of synthesized NPs were analyzed using Scanning Electron Microscope Hitachi, S-3400N, Japan. The EDS using Thermo fisher scientific, Noran System 7, the USA for identifying elements. The Size, Shape, d-spacing and SAED pattern of synthesized NPs were analyzed at 200KV, CMOS Camera 4K×4K using Transmission Electron Microscope TALOS F200S G2. The ultrasonic bath was used to disperse the synthesized material by sonication.

Results and discussion

Optical properties of synthesized nanoparticles

Nanomaterials having small particle sizes exhibit enhanced optical emission as well as nonlinear optical properties. Nanoparticles made of semiconductor materials, absorb and emit light at certain wavelengths that depend strongly on particle size and shape due to quantum confinement effects.

UV-Visible Spectroscopy

UV-Visible absorption spectroscopy is the technique for preliminary confirmation of synthesized nanoparticles. The unique surface Plasmon resonance (SPR) property of noble metals strongly induces the absorption of the incident light and it can be monitored by UV-visible spectroscopy.

In this work, the biosynthesized ZnO showed a strong Surface Plasmon Resonance (SPR) peak at 365nm and Ag-ZnO gives a peak at 372nm and a new peak at 415nm corresponds to the Ag on to the surface of ZnO [11] **Fig. 1**. The broadness of the peak is due to the oscillations of Plasmon from Ag atoms and its clustering on the surface of ZnO. No structural alteration is observed on the addition of Ag to ZnO, the peak corresponding to that of ZnO is shifted to a longer wavelength with the addition of Ag dopant which probably may result in a decreased energy gap.
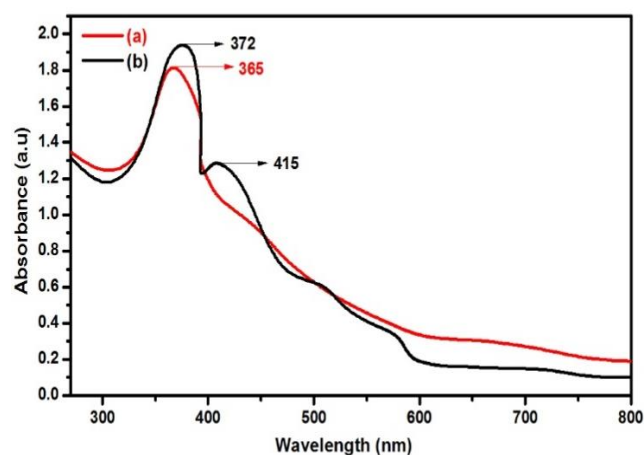
Fig.1. UV-visible spectra of **(a)** ZnO and **(b)** Ag-ZnO Nanocomposites.

Energy band gap analysis

The optical parameters of the prepared nanocomposites are measured using a UV-visible spectrometer in the operating range of 300-800 nm. UV-Visible spectra serve as an optimal tool for measuring the bandgap.

The energy difference between the valence band and conduction band is termed as bandgap which plays an important role in optimizing the optical properties of any solid materials. The UV-visible spectra of ZnO and Ag-ZnO nanocomposites are shown in **Fig. 1**. ZnO shows a strong absorption band 372 nm, corresponding to a wurtzite crystal structure of the ZnO. By doping the Ag, the absorption maximum moved towards the longer wavelength. The change in the wavelength corresponding to maximum absorption will certainly lead to the change in the band structure, further resulting in the change in the energy gap.

The optical energy band gap of ZnO and Ag-ZnO nanocomposites are calculated using Tauc's relation [30,31].

$$\alpha h\nu = A\left(h\nu E_g\right)^n \qquad (1)$$

where, E_g is the bandgap energy, α is the optical the absorption coefficient, $h\nu$ is the energy of an incident photon, A is the proportionality constant depends on the transition probability and n=2 for indirect transition [32,33]. Using the Kubelka-Munk transformation equation we plotted the graph of $(\alpha h\nu)^2$ Vs $h\nu$ and extrapolating the graph onto the photon energy axis as shown in **Fig. 2**.
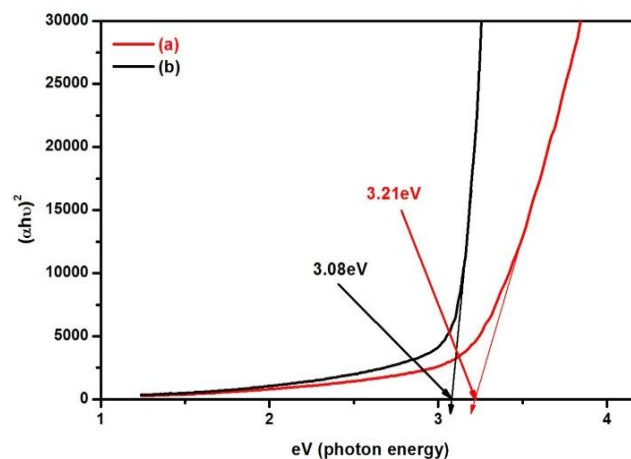
Fig.2. Tauc's plot for the calculation of energy band gap for **(a)** ZnO and **(b)** Ag-ZnO nanocomposites.

The E_g of Biosynthesized ZnO nanoparticles were found to be 3.21eV, which is decreased to 3.08eV after doping the Ag. The decrease in the energy gap value is mainly due to the dopant and E_g may also depend on size and shape of the nanoparticles. The acceptor impurity results decrease in the energy gap. The electrons from the valance band are excited to the conduction band by moving through the Fermi levels of the Ag clusters.

**Advanced
Materials Letters**
www.vbripress.com/aml

IAAM®
Advancement of Materials
to Global Excellence

www.iaamonline.org
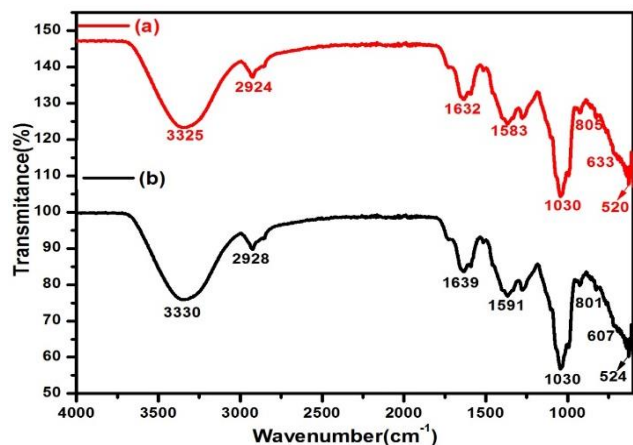
Fig. 3. FT-IR spectra of biosynthesized (**a**) ZnO & (**b**) Ag-ZnO nanocomposites.

Fourier Transform Infrared Spectroscopy (FTIR)

The FTIR spectroscopy gives the details of different functional groups involved in the stabilization, reducing agent, and capping agent for the nanoparticles. FTIR spectrum of biosynthesized ZnO is shown in **Fig. 3(a)**. A broad peak at 3325 cm^{-1} and 3330 cm^{-1} shows the OH stretching vibrations. The 2924 cm^{-1} and 2928 cm^{-1} peak reveals the NH bending, the moderate peaks at 1632cm^{-1}, 1639 cm^{-1}, 1591 cm^{-1} and 1583 cm^{-1} are witnessing the carboxylic group. The sharp peak was observed at 1030 cm^{-1} which corresponds to CO stretching and CH phase bending was observed at 805 cm^{-1} and 801 cm^{-1}. The peak was also observed at 633 cm^{-1} and 607 cm^{-1} which corresponds to N-containing bio ligands [**34**]. A characteristic vibrational mode for ZnO appeared at 520 cm^{-1} and 524 cm^{-1} for Ag-ZnO as shown in **Fig. 3(b)**.

After the deposition of Ag on the surface of ZnO NPs, the relative intensities of ZnO gets decreased with slight shifts to the higher frequencies this possible reduction of Ag ion is due to biomaterials [**35**].

Powder X-Ray diffraction studies

The XRD pattern of ZnO and Ag-ZnO is shown in **Fig. 4**. The spectrum which is in good agreement with JCPDS file 36-1451and 04-0783 respectively, the prepared composites are polycrystalline in nature and face-centered cubic structure. The spectra for ZnO shows an intense peak at 37.98° corresponding to (002) and found to be unaltered in the spectra of Ag-doped ZnO, suggests that the Ag does not induce any imperfections in the ZnO crystallites. Also, the peaks at 29.08° and 44.43° corresponding to (100) and (200) respectively, the peak indicates the Ag phaseand a little broadness appeared in its spectra due to the clustering of Ag. With this we also obtained wide blunt peaks around 64° the **Fig. 4(b)** that is due to presence of Ag. The intensity of the XRD peaks is improved on the addition of Ag, indicating that the crystallinity of the nanocomposites are enhanced by the addition of dopant Ag[**35,36**].

The synthesized nanoparticles were crystalline in nature which is confirmed by the XRD data and they had a hexagonal wurtzite phase [**37,38**]. Further, the average crystallite size of biosynthesized ZnO and Ag-ZnO was calculated using the Debye-Scherrer formula:

$$D = \frac{k\lambda}{\beta Cos\theta} \qquad (2)$$

where, **D** is crystallite size, **k** = 0.9 is the shape factor, λ is the X-ray wavelength of Cu **Kα** radiation (1.54 Å), θ is the Bragg diffraction angle, and β is the full width at half maximum of the (002) plane diffraction peak.

The calculated average crystallite size was estimated to be 120.16nm and 91.17nm for ZnO and Ag-ZnO respectively.
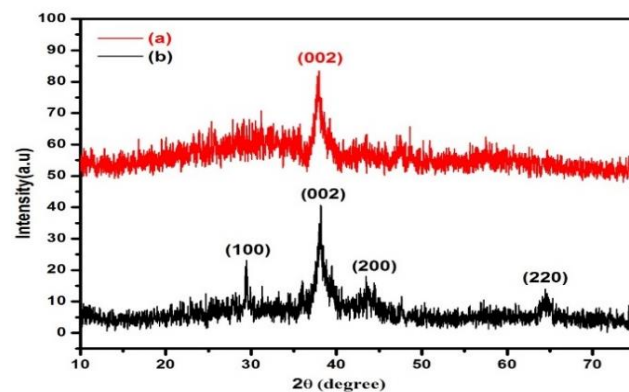
Fig. 4. XRD spectra of biosynthesized (**a**) ZnO and (**b**) Ag-ZnO nanocomposites.

Scanning Electron Microscopy (SEM)

SEM provides insight into the morphology and size details of the synthesized nanocomposites. The SEM images of biosynthesized ZnO and Ag-ZnO nanocomposites are shown in **Fig. 5**. It can be seen from **Fig. 5(a)**, that layer like hexagonal morphology for ZnO crystallites and **Fig. 5(b)** shows distinct plates and spherical like heterostructures of Ag-ZnO, where Ag is deposited over ZnO crystallites [**15**].

In **Fig. 5(b)** we can observe the agglomeration in distribution of nanocomposites and decrease in particles size. That may due to the interaction of silver Nanoparticles with ZnO. The average grain size was calculated using the linear intercept method and was found to be around 128nm for ZnO and around 90nm for Ag-ZnO. The results showed that the nanoparticles are spherical in shape and are deposited above the rod-shaped structure.
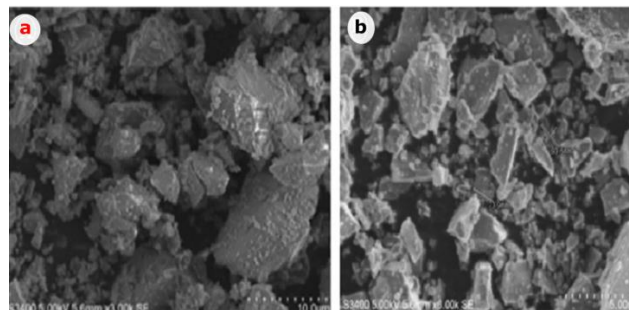
Fig. 5. SEM images of (**a**) ZnO and (**b**) Ag doped ZnO nanocomposites.

Energy Dispersive X- Ray Studies (EDS)

The energy dispersive X-Ray spectroscopy was applied to distinguish the elemental composition between the spherical architecture of ZnO and Ag-ZnO. **Fig. 6(a)** and **Fig. 6(b)** show Energy Dispersive X-Ray Studies of nanoparticles without dopant (ZnO) and with a dopant (Ag-ZnO).
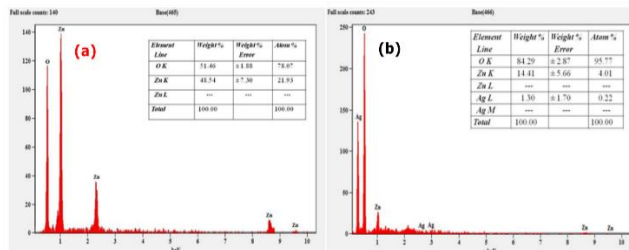
Fig. 6. EDS Spectra of (**a**) ZnO and (**b**) Ag-ZnO nanoparticles.

The EDS spectra revealed the presence of ZnO and Ag elements in the synthesized nanoparticles. The data of EDS has been tabulated in the inset of EDS spectra **Fig. 6**. In the **Fig. 6(a)** we observed only one peak with weight % Zn-21% and O-78%. This shows that the synthesized nanoparticles are pure ZnO. **Fig. 6(b)** showed the two intense peaks related to ZnO and Ag. Here we did not observe any impurities the peak with weight % of 95 %, 4% and 0.22% represents the element of O, Zn & Ag respectively.

Transmission Electron Microscopy (TEM)

Fig. 7 depict the TEM images of ZnO and Ag-ZnO nanoparticles, the **Fig. 7(a1)** and **Fig. 7(b1)** indicates flakes and different size spherical heterostructures with agglomeration corresponding to ZnO and Ag-ZnO Nanoparticles. Average size anchored by ZnO and Ag-ZnO nanoparticles was in the range of 84.88 nm and 119.66 nm respectively. **Fig. 7(a2)** and **Fig.7(b2)** shows the 0.30nm and 0.51nm d-spacing in lattice fringes with respect to (002) and (100) planes [**39,40**]. From the **Fig. 7(a3)** and **Fig. 7(b3)** shows the SAED pattern of ZnO and Ag-ZnO nanoparticles, the bright spot in the SAED pattern indicates the sample is well crystallized in nature.
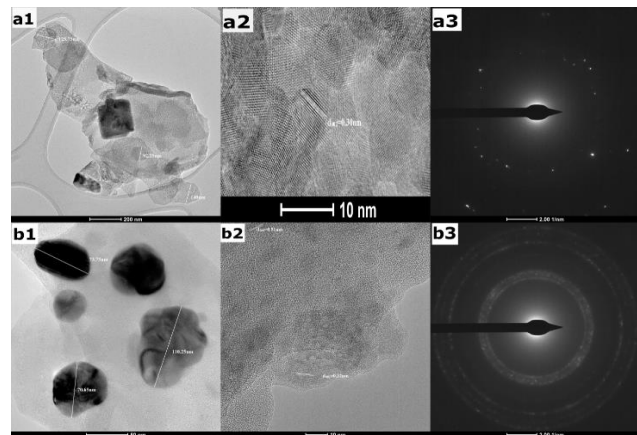
Fig. 7. a1 & b1. TEM images of ZnO and Ag-ZnO nanoparticles, a2 & b2. nanoparticles showing Bragg's planes and a3 & b3. SAED images of ZnO and Ag-ZnO nanoparticles.

Dynamic Light Scattering (DLS) analysis

Dynamic Light Scattering is one such reliable technique for determining particle size and their distribution in solution [**41**]. The DLS analysis of synthesized nanocomposites is in **Fig. 8**.
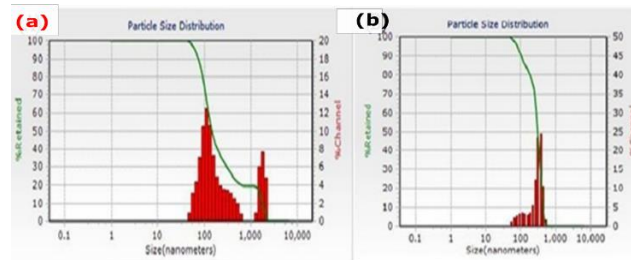
Fig. 8. Particle size distribution of (**a**) ZnO and (**b**) Ag-ZnO nanocomposites.

The distribution range of particles approximately is in the range of 50nm to 650 nm. Thus, ZnO is obtained with an average size of 125.4 nm diameter and that of Ag-ZnO with an average size of 92.8 nm diameters as shown in **Table 1**. Also, from the graph, the nanocomposites of various sizes are found, and the result agrees with that of SEM analysis too.

Table. 1. Dynamic light scattering results of ZnO and Ag-ZnO nanoparticles.

ZnO			Ag-ZnO		
Diameter (nm)	Volume (%)	Width	Diameter (nm)	Volume (%)	Width
125.4	80.9	197.8	92.8	15.2	54.2

By comparing the above two results, we can conclude that metal oxide with dopant is very appropriate since it gives the lowest average size of nanoparticles.

Evaluation of the antimicrobial activity of Zinc Oxide nanoparticles

Antibacterial activity

The ZnO & Ag-ZnO nanoparticles were screened for antibacterial activity against Gram-positive bacteria *B.subtilis, Streptococci strains* and negative strain *E.coli* along with streptomycin were carried out by disc diffusion method [**41,42**].
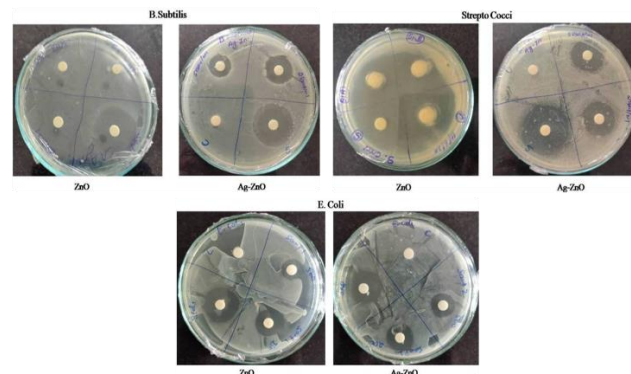
Fig. 9. The Antibacterial activity of ZnO and Ag-ZnO was evaluated against *B.subtilis, Streptococci*, and *E.coli* by Disk Diffusion Method.

Test bacteria were seeded evenly onto the surface of nutrient agar (NA)media maintaining a concentration of 1.5×10^8 CFU ml^{-1} using a sterile glass spreader. The sterile discs (6 mm) were loaded with 50μL of ZnO and Ag-ZnO in 500μg/ml and 250μg/ml concentration to each disc and placed on agar plates along with standard streptomycin. The inoculated plates were incubated for 24 h at $37 \pm 2°C$ and the zone of inhibition was measured around the discs. All the different concentrations of ZnO and Ag-ZnO nanoparticles are prepared with sterile distilled water. The experiment was repeated in triplicates along with standard. The inhibitory efficacy of ZnO and Ag-ZnO nanoparticles against *B.subtilis, Streptococci* and *E.coli* is shown in **Table 2**.

Table 2. Zone of inhibition of ZnO and Ag-ZnO against *B.subtilis, Streptococci* and *E.coli*.

Organism	Zone of inhibition in (mm) at 250 µg/disc					
	ZnO			Ag-ZnO		
	Std (in mm)	500 µg/ml (in mm)	250 µg/ml (in mm)	Std (in mm)	500 µg/ml (in mm)	250 µg/ml (in mm)
B.subtilis	15±1.2	……	……	15±0.5	*12±1.5	*8±0.6
Streptococci	14±0.5	-----	------	16±0.7	11±0.6	*9±0.6
E.coli	12±0.5	*6±0.3	*6±0.5	11±0.4	*8±0.3	*9±0.5

*All the Values are represented in Mean ± SEM, n=2, *p>0.05 is compared to Std.*
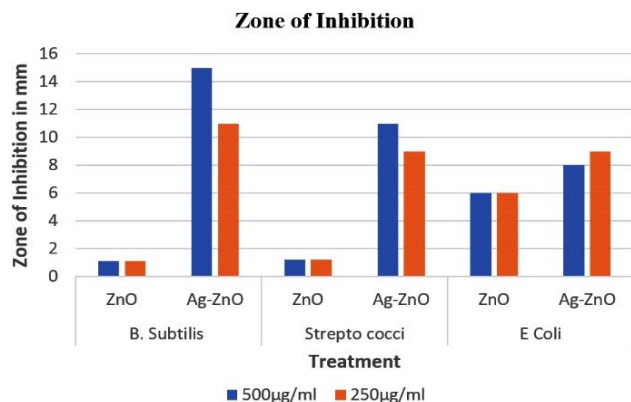
Fig. 10. Zone of inhibition of ZnO and Ag-ZnO against *B.subtilis, Streptococci* and *E.coli*.

Among the tested bacteria, susceptibility was recorded higher in *B.subtilis, Streptococci* and *E.coli* with Ag-ZnO. Both 500 µg/ml and 250 µg/ml of Ag-ZnO showed significant results compared to standard **Fig. 10**.

On injecting the ZnO and Ag-ZnO nanoparticles on the bacteria, it leads to damage in DNA, cell membranes due to reactive oxygen species (ROS) mechanism as shown in **Fig. 11**. Direct interaction occurs with cell membranes due to the presence of metal ions in the synthesized materials [**32**]. It has also shown excellent activity and tested for MICs 62.5 µg/ml, however, P. Amornpitoksuk *et. al.,* reported with MICs 512 µg/ml [**43**].
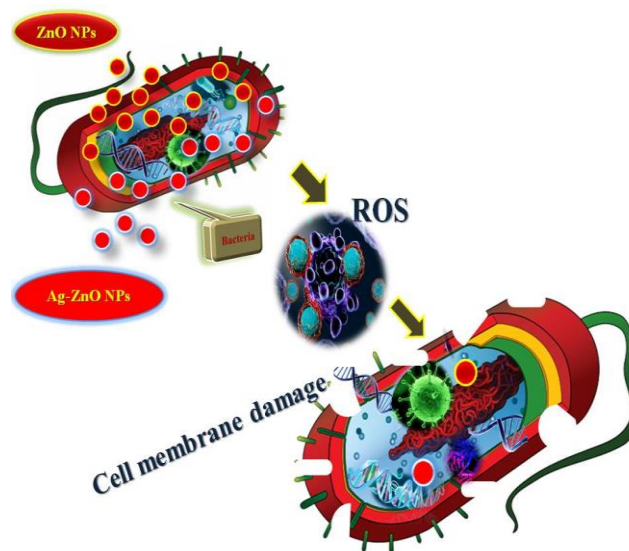
Fig.11. Mechanism of ZnO and Ag-ZnO nanoparticles towards antibacterial activity.

Minimum inhibitory concentration determination of ZnO and Ag-ZnO

Methodology

The antibacterial activity of the ZnO and Ag-ZnO nanoparticles was determined using sterile 2ml 96-well plates against *B.subtilis, Streptococci* and *E.coli* The 12 wells of each row were filled with 150µl of sterilized Mueller Hinton agar as a blank, Sequentially, wells 2–11 received an additional 150µl of a mixture of culture medium served as control and well 3-11 received ZnO nanoparticles in different concentration of 1000, 500, 250, 125 and 62.5µg/ml, as same for Ag-ZnO in different concentration (1000, 500, 250, 125 and 62.5µg/ml) was loaded to well 6,7,8-11 and incubated at $37 \pm 2°C$ for 24hrs. 10µl of Resazurin die was added to each well and incubate for 4hrs.

Absorbance was measured at 620nm without agitation using ELISA plate reader (Lab Tech 4000). The experiment was repeated in duplicates along with standard. MIC value for both ZnO and Ag-ZnO was evaluated against the three bacterial strains *B.subtilis, Streptococci* and *E.coli* were done by serial dilution method. Ag-doped ZnO 1000 µg/ml and 500µg/ml showed the highest inhibition when compared to ZnO in all three strains. Ag-ZnO showed concentration-dependent inhibitory activity against *B.subtilis, Streptococci* and *E.coli* as in **Fig. 10**. ZnO didn't show promising inhibitory activity against *B.subtilis, Streptococci* when compared to Ag-ZnO **Table 2**. Whereas, pure Zn, as well as Ag-ZnO both, are having activity against the *E.coli*, but 1000µg/ml concentration of Ag-ZnO showed the highest inhibitory(approximately 70%) activity when compared to ZnO in *E.coli*. Therefore, Ag-ZnO is having significant inhibitory activity against all the bacterial strains.

Conclusion

In the present investigation, aqueous extracts of leaves of *Macrotyloma Uniflorum* is successfully used for green synthesis of ZnO and Ag-ZnO nanoparticles. The synthesized nanocomposites were subjected to spectral characterization. The UV-Visible absorption spectral analysis offered a peak at 365nmfor ZnO and in the Ag-ZnO peaks at 372nm and 415nm characteristic to Ag nanoparticles. The optical absorption measurements indicated a decreased bandgap after Ag inclusion as a p-type dopant, and play a significant role in its use in optoelectronic industry. The FTIR spectroscopy indicated the compounds present in the plant extract complexes well to form a metal oxide, and the biomolecules act as a reducing and or capping agent and help further in the stabilization of the nanocomposites. The XRD, TEM and DLS analysis confirmed the size of particles were at the average 91.17 nm for with dopant and 120.16 nm for bare ZnO. SEM and TEM analysis show the flakes like hexagonal morphology for ZnO crystallites and Ag-ZnO shows different size spherical heterostructures with agglomeration. The EDS confirmed the bio-fabricated ZnO and Ag-ZnO nanocomposites. SAED pattern of TEM confirmed the crystallized nature of nanoparticles. Synthesized nanoparticles have shown excellent antibacterial activity against gram bacteria for various concentrations. MIC value of antibacterial activity against ZnO and Ag-ZnO nanoparticles is 62.5 µg/ml. Based on all above work, the green synthesized Ag-ZnO nanoparticles proved that they are good at antibacterial activities.

References

1. Rüdiger, S.K.; Groß, U.; Feist, M.; Prescott, H.A.; Shekar, S.C.; Troyanov, S.I.; Kemnitz, E.; J*ournal of Materials Chemistry*, **2005**, *15,* 588.
2. Kim, T.W.; Ha, H.; Paek, M.; Hyun, S.; Choy, J.; Hwang, S.; *Journal of Materials Chemistry,* **2010**, 3238.
3. Bonilla, C.A.M.; Kouznetsov, V.V.; Green Nanotechnology - Overview and Further Prospects, **2016**, 2-20.
4. Thorne, R.J.; Nicholson, C.; Proceedings of the National Academy of Sciences of the United States of America, **2006**, *103,* 5567-72.
5. Nath, D.; Banerjee, P.; *Environmental Toxicology and Pharmacology,* **2013**, *36,* 997.
6. Darroudi, M.; Sarani, M.; Kazemi Oskuee, R.; Khorsand Zak, A.; Amiri, M.S.; *Ceramics International,* **2014**, *40,* 2863.
7. Palmqvist, A.E.C.; *Curr. Opin. Colloid Interface Sci,* **2003**, *8,* 145.
8. Ruparelia, J.P.; Chatterjee, A.K.; Duttagupta, S.P.; Mukherji, S.; *Acta Biomaterialia,* **2008**, *4,* 707.
9. Huo, C.; Ouyang, J.; Yang, H.; *Scientific Reports, Nature,* **2014**, 1-9.
10. Siavash, I.; *Green Chemistry,* **2011**, 2638-2650.
11. Jadhav, S.; Gaikwad, S.; Nimse, M.; Rajbhoj, A.; *J. Clust. Sci,* **2011**, 121.
12. Ford, P.C.; Cariati, E.; Bourassa, J.*; Chemical Reviews,* **1999**, *99,* 3625.
13. Janotti, A.; Van De Walle, C.G.; *Rep. Prog. Phys,* **2009**, *72,* 126501.
14. Mai, W.; Synthesis, characterization and application of ZnO nanomaterials, **2009**, 139.
15. Sun, Y.; Chen, L.; Bao, Y.; Zhang, Y.; Wang, J.; Fu, M.; Wu, J.; Ye, D.; *Catalysts,* **2016**.
16. Bharathi, D.; Vasantharaj, S.; Bhuvaneshwari, V.; IOP Publishing Ltd, **2018**.
17. Bharathi, D.; Bhuvaneshwari, V.; *Research on Chemical Intermediates,* **2019**, *45,* 2065.
18. Hunagund, S.M.; Desai, V.R.; Kadadevarmath, J.hS.; Barretto, D.A.; Vootla, S.; Sidarai, A.H.; *RSC Advances,* **2016**, *6,* 97438.
19. Bar, H.; Bhui, D.K.; Sahoo, G.P.; Sarkar, P.; De, S.P.; Misra, A.; *Physicochemical and Engineering Aspects*, **2009**, *339,* 134.
20. Parashar, V.; Parashar, R.; Sharma, B.; Pandey, A.C.; *Digest Journal of Nanomaterials and Biostructures,* **2009**, *4,* 45.
21. Tharani, S.; Bharathi, D.; Ranjithkumar, R.; Biocatalysis and Agricultural Biotechnology, **2020**.
22. Bhartiya, A.; Aditya, J.P.; Kant, L.; *The Journal of Animal & Plant Sciences,* **2015**, *25,* 908.
23. Kumar, P.; Kumar, R.; Kumar Sinha, R,R.; *IJLPR,***2020**,11, L80.
24. Seneviratne, K.N.; HapuarachchI, C.D.; Ekanayake, S.; *Food Chemistry,* **2009**, *114,* 1444.
25. Kavitha, K.; Baker, S.; Rakshith, D.; Kavitha, H.; Yashwantha Rao, H.; Harini, B.; Satish S.; *Int. Res. J. Biological Sci.,* **2013**, *2,* 66.
26. Patil, P.N.; Sawant, D.V.; Deshmukh, R.N.; *Int. J. Envt. Sci,* **2012**, *3,* 1194.
27. V, J.L.; Sharath, R.; Mn, C.; Neelufar, E.; Hazra, A.; Patra, M.; *J. Biochem Tech.,* **2012**, *3,*151.
28. Gunalan, S.; Sivaraj, R.; Rajendran, V.; *Materials International,* **2012**, *22,* 693.
29. Khac, V.; Bui, H.; Park, D.; Lee, Y.; A Mini Review of the Research Trends, Polymers, **2017**.
30. Pujar, M.S.; Hunagund, S.M.; Sali, R.K.; AIP Conference Proceedings, **2019**, 020075.
31. Jadhav, M.S.; Kulkarni, S.; Raikar, P.; Barretto, D.A.; Vootla, S.K.; Raikar, U.S.; *New Journal of Chemistry,* **2018**, *42,* 204.
32. Sali, R.K.; Pujar, M.S.; Nadgir, A.; Ashok, A.H.; AIP Conference Proceedings, **2020**, *070024,* 2-6.
33. Pujar, M.S.; Hunagund, S.M.; Barretto, D.A.; Desai, V.R.; Patil, S.; Vootla, S.K.; Sidarai, A.H.; *Bulletin of Materials Science,* **2020**, *43,* 24.
34. Coates, J. A.; Encyclopedia of Analytical Chemistry, **2000**, 10815-10837.
35. Ghosh, O.S.N.; Sudhakara, P.; Ray, S.S.; Africa, S.; Viswanath, K.; *Applied Science Letters,* **2015**, *1,* 8.
36. Choudhary, M.K; Kataria, J.; Bhardwaj, V.K.; Sharma, S.; *Nanoscale Advances,* **2019**, *2,* 1.
37. Zeferino, R.S.; Barboza-flores, M.; Pal, U.; *J. Appl. Phys.,* **2011**.
38. Shanmugam, S.; Soga, T.; *J. Appl. Phys,* **2015**, *109,* 014308.
39. Hao, Lu.; Kaimo, Deng.; Zhiwei Shi Qiong, Liu.; Guobin, Zhu.; Hongtao, Fan.; Liang, Li.; *Nanoscale Research Letters,* **2014**, *9,* 183.
40. Xu, Liu.; Weibo, Li.; Nan, Chen.; Xinxin, Xing.; Chenjun, Don.; Yude, W.; *RSC Advances,* **2015**, *10,* 39.
41. Ghorbani, H.R.; Rashidi, R.; *Journal of Pure and Applied Microbiology,* **2015**, *9,* 1747.
42. Meruvu, H.; Vangalapati, M.; Chaitanya Chippada, S.; Rao Bammidi, S.; *Rasayan Journal of Chemistry,* **2011**, *4,* 217.
43. Amornpitoksuk, P.; Suwanboon, S.; Sangkanu, S.; Sukhoom, A.; Muensit, N.; Baltrusaitis, J.; *Powder Technology,* **2012**, *219,* 158.